Composites Part C: Open Access 5 (2021) 100139

Contents lists available at ScienceDirect

Composites Part C: Open Access

journal homepage: www.elsevier.com/locate/jcomc

Fatigue and fatigue after impact behaviour of Thin- and Thick-Ply composites observed by computed tomography

Benedikt Kötter[a,*], Janina Endres[a], Johann Körbelin[a], Florian Bittner[b], Hans-Josef Endres[b], Bodo Fiedler[a]

[a] Hamburg University of Technology, Institute of Polymer and Composites, Denickestraße 15, Hamburg 21073, Germany
[b] Leibniz University Hannover, Institute of Plastics and Circular Economy (IKK), An der Universität 2, Garbsen 30823, Germany

ARTICLE INFO

Keywords:
Low-velocity impact
Delamination
Damage progression
Load ratio
Constant-life diagram

ABSTRACT

This study investigates the influence of load ratio and impact damage on the fatigue behaviour of high-performance carbon fibre reinforced polymers (CFRP) with areal fibre weights between 30 gsm and 360 gsm. For undamaged samples, the ultimate tensile and compressive strength, as well as the fatigue properties, are evaluated with regard to their layer thicknesses. The fatigue tests were performed under tension-tension (R=0.1), tension-compression (R=-0.5) and compression-compression (R=10) regime. The results are illustrated as a constant-life diagram, and a piecewise linear interpolation examines a first prediction. The results show that static and fatigue performance improves with decreasing layer thickness. Particularly under tension-compression loading, significant improvements are observed, due to the suppression of matrix cracks and delaminations with thinner layers. In addition, the effect of low-energy impact on the fatigue behaviour of Thin- and Thick-Ply laminates is investigated. The tests demonstrate that although the delamination area is larger, Thin-Ply laminates can sustain higher stresses and still reach the same number of load cycles in contrast to Thick-Ply laminates. Computed tomography measurements visualize 3-dimensional the damage progression after various cycles and prove that the Thin-Ply composites show no increase in the damaged area during fatigue. The interlaminar stress at the delamination is not sufficient for expansion. In contrast, in the case of thicker layers, the damage growths progressively throughout the whole sample with increasing number of cycles.

1. Introduction

Fatigue and impact tests are of particular interest in the design process of structural components. Fatigue tests are utilised to determine the lifetime of a material under different load ratios, and low-velocity impact tests represent critical damage to the structure [1]. Defects in laminated composite structures like voids and impact damages have a major influence on the fatigue behaviour [2,3]. Due to their lightweight performance, carbon fibre reinforced polymers are increasingly used. However, their impact tolerance, lifetime and failure behaviour differs significantly from conventional construction materials such as metals [4]. The behaviour of fibre reinforced polymers (FRP) is complex. For example, the impact causes inter-fibre fractures, delaminations and, depending on the energy applied, fibre breakages. The defects are distributed within the material, whereby the damage pattern's size and shape depend on several factors. These include, for example, the properties of the samples to be tested, such as stiffness and layer structure, the clamping system used and the applied impact energy. The detection of such damage is difficult. Here, methods such as ultrasonic examination, active thermography or computed tomography are used [2,5–8]. Studies show that impact damage can reduce the load-bearing capability of CFRP by up to 50% under tensile load [9]. Fibre composites also exhibit complex failure behaviour under cyclic load. In contrast to metals, where one critical crack forms, grows and leads to final failure, FRPs have a complex delamination dominant failure behaviour. At a low stress level or numbers of load cycles, the relatively low strength of the matrix leads to inter-fibre fractures, which form in the 90° layer perpendicular to the load direction. Delaminations are initiated with the increasing length of the cracks and the associated high stresses at the crack tip. Earlier studies showed that the damage progression is associated with a decrease in Young's modulus [10–13]. The material fails prematurely below the nominal elongation of the fibres. The full potential of the fibres cannot be exploited. Premature failure leads to a conservative component design [14]. Defects in laminated composite structures like voids and impact damages have a major influence on the fatigue behaviour [15].

One approach to increase the performance of FRPs is to reduce the layer thickness. Studies by Kawabe et al. and Sihn et al. [16,17] describe a roving spreading process, allowing conventional rovings to be used for

* Corresponding author.
E-mail address: benedikt.koetter@tuhh.de (B. Kötter).

https://doi.org/10.1016/j.jcomc.2021.100139
Received 4 February 2021; Received in revised form 22 March 2021; Accepted 22 March 2021

thin layer thicknesses of up to 20µm. Usually, layer thicknesses below 60µm are described as Thin-Ply materials. Using thinner layers, the manufacturing of thinner laminates is possible, and the freedom in design of the lay-up is increased [18–21]. Regarding the mechanical failure behaviour, the failure mechanisms of undamaged samples change from complex delamination dominated to brittle failure and pre-damage is reduced with decreasing layer thickness. Due to the suppression of pre-damage, the stiffness of the specimens does not decrease under load [22]. Yokozeki et al. [23] showed by acoustic emission tests that the initiation of damage shifts to higher strains and thus higher stresses. Furthermore, the number of inter-fibre fractures at lower stresses decreases with decreasing layer thickness and can be explained by the so-called "in-situ strength", whereby the transverse strength of the matrix increases with decreasing layer thickness. The in-situ strength has been investigated in detail in many studies [24–26]. Saito et al. [27] showed that the energy at the crack tip is highest at a length of 75% of the layer thickness because the neighbouring layers suppress the crack-opening. The energy of shorter cracks is not sufficient to initiate delaminations, and therefore, they are suppressed. Even under compressive load, the strength is improved. Laminate quality, lay-up and failure behaviour have a positive influence on the compressive strength. Resin-rich regions and voids are smaller, and the fibres are more homogeneous distributed due to the spreading process [18,20]. According to the literature, six parameters are most important for investigating fatigue behaviour of fibre reinforced composites. These include the loading pattern, the control mode, the stress ratio, strain rate, waveform and the temperature [28]. In the case of Thin-Ply samples, a seventh factor, the layer thickness, is acknowledged. Sihn et al. and Yamaguchi et al. investigated Thin-Ply laminates under fatigue loading (tension-tension). The samples performed as if under static tensile load. They showed an increased lifetime, a smaller decrease in stiffness reduction and exhibit a brittle failure [17,29].

To estimate the influence of different load ratios on the fatigue lifetime of a material for which no experimental data is available, constant-life diagrams (CLD) are a fast and powerful tool. Especially in fields where few fatigue investigations have been carried out, as is the case with Thin-Ply CFRP materials and the samples expensive to manufacture, CLDs represent an excellent first approximation. The main parameters defining a CLD are the mean cyclic stress, the cyclic stress amplitude and the load ratio (R-ratio) as the quotient between the minimum and maximum cyclic stress. Depending on the material behaviour, different interpolation approaches can be chosen. The simplest type of interpolation is the linear CLD model, which only requires one S-N curve resp. Wöhler curve, but assumes that the material behaves the same under tensile and compressive loads [28]. Different approaches were proposed, which can be used depending on the examined material behaviour. The most commonly used non-linear interpolation approaches include Harris's CLD [30], Kawai's CLD [31], Boerstra's CLD [32], and Kassapoglou's CLD [33]. Within this study, the piecewise linear interpolation [34] is used. The piecewise linear interpolation model requires a limited number of S-N curves and the ultimate tensile and compressive strength. For most of the composite studies, the predictions based on piecewise linear interpolation are the most accurate [28].

Philippidis et al. proposed an analytical description of the piecewise linear interpolation method for the individual regions of the CLD, enabling unknown load ratios (R') to be calculated [34]. If R' is in the tensile-tensile region and between $R = 1$ and the first known measured value (R_{1TT}) counterclockwise, formula 1 applies.

$$\sigma'_a = \frac{UTS}{\frac{UTS}{\sigma_{a,1TT}} + r' - r_{1TT}} \tag{1}$$

σ'_a displays the interpolated and $\sigma_{a,1TT}$ the experimental determined amplitude stresses and UTS the ultimate tensile strength. The further parameters are calculated according by $r_i = (1 + R_i)/(1 - R_i)$ and $r' = (1 + R')/(1 - R')$. In the first case, $R_i = R_{1TT}$ applies.

If R' is between two known R-ratios, R_i and R_{i+1}, formula 2 applies.

$$\sigma'_a = \frac{\sigma_{a,i} \cdot (r_i - r_{i+1})}{(r_i - r') \cdot \frac{\sigma_{a,i}}{\sigma_{a,i+1}} + (r' - r_{i+1})} \tag{2}$$

If R' is in compressive-compressive region and clockwise between $R = 1$ and the first measured value in compressive region, R_{1CC}, formula 3 applies. UCS represent the ultimate compressive strength.

$$\sigma'_a = \frac{UCS}{\frac{UCS}{\sigma_{a,1CC}} - r' + r_{1CC}} \tag{3}$$

In the case of Thick-Ply FRPs, several studies have investigated the fatigue after impact (FAI) behaviour. Delaminations significantly reduce the lifetime [35–37]. At the same time, studies on impact damage of Thin-Ply show that the delamination areas increase with thinner layers [18,38]. In combination with the larger delamination area, the impact behaviour could be a limiting factor using Thin-Ply structures. However, previous studies show that under tensile and compressive loading of undamaged samples, less damage is initiated with decreasing layer thickness and existing damage grows more slowly [17,18,39]. This can have positive effects on the cyclic performance of structures damaged by an impact. For this reason, the cyclic behaviour of impacted samples is investigated as a function of the layer thickness.

2. Materials and and methods

2.1. Materials and specimen preparation

The material used in this study is a CFRP unidirectional prepreg system produced by NTPT (North Thin Ply Technology, Switzerland), which is composed of NTPT's epoxy resin TP402 and T700S carbon fibres from Toray Carbon Fibers America, Inc. The target for the fibre volume content of the prepregs was 55%. The produced fibre area weights are 30 gsm, 60 gsm and 120 gsm. Higher fibre area weights such as 240 gsm and 360 gsm were produced by block-scaling an according to the number of same-oriented layers. The prepregs were cut by CNC cutter (Aristomat TL1625 from ARISTO Graphic Systeme GmbH & Co. KG i.I., Germany) and manufactured by hand lay-up. The layers were debulked by a vacuum bag every fourth layer. Table 1 shows the used lay-ups. The curing of the laminates was according to the process suggested by the manufacturer NTPT. The maximum temperature was 160°C, and the differential pressure was 7bar. The cured laminates were sawn using ATM's Brilliant 265 precision saw with a corundum blade at a feed rate of 1.5mm/s. Depending on the test method, tabs were bonded on the samples before cutting, to reduce stress concentrations in the load introduction area and thus prevent premature failure. In the case of tensile samples and the fatigue samples, which are loaded under tension-tension (R=0.1), a combination of ±45° lay-up, 1mm thick GFRP and 1mm thick aluminium tabs were used. For the compression tests and fatigue compression-compression (R=10) tests, the used tab material was a ±45° lay-up GFRP laminate with a thickness of 2mm. In both cases, the tabs are bonded at 80° C with the epoxy resin adhesive UHU Endfest plus 300 from UHU GmbH & Co. KG, Germany. The specimen dimensions of the tensile and compression tests correspond to the ASTM standards used. The fatigue tests samples under tensile-tensile load (R=0.1) have the same geometry as the samples for the static tensile tests. An exception is the 30 gsm samples. Due to the stress concentrations in load introduction area in connection with the damage suppression behaviour of the thin layers, non-standard failures occur in the area of the load introduction. To achieve a standard-conforming failure, a CNC milling machine (Isel EuroMod MP30 from isel Germany AG, Germany) milled the samples to the shape of a dogbone. The gauge length is 130mm and the gauge width 21 mm. The specimens for the cyclic tests under tensile-compressive load also correspond to the geometry of the static tensile tests. Depending on the buckling support used, tabs are used or not. The buckling supports are explained in more detail in the following

Table 1
Laminate lay-ups.

	Fibre areal weight in gsm				
Test Method	30	60	120	240 (2x120)	360 (3x120)
Tension	$[45/90/-45/0]_{12s}$	$[45/90/-45/0]_{6s}$	$[45/90/-45/0]_{3s}$	$[45_2/-45_2/90_2/0_2]_s$	$[45_3/90_3/-45_3/0_3]_s$
Compression	$[45/90/-45/0]_{22s}$	$[45/90/-45/0]_{11s}$	$[45/90/-45/0]_{6s}$	$[45_2/90_2/-45_2/0_2]_{3s}$	$[45_3/90_3/-45_3/0_3]_{2s}$
Fatigue	$[45/90/-45/0]_{12s}$	$[45/90/-45/0]_{6s}$	$[45/90/-45/0]_{3s}$	–	$[45_3/90_3/-45_3/0_3]_s$
FAI	$[45/90/-45/0]_{12s}$	$[45/90/-45/0]_{6s}$	$[45/90/-45/0]_{3s}$	–	$[45_3/90_3/-45_3/0_3]_s$

Table 2
Test Methods and specimen dimensions (*Tension-Compression 30 gsm no tabs, **Tension-Tension 30 gsm).

Specimen Dimension	Tension ASTM D3039-00	Compression ASTM D3410-03	Fatigue after Impact –
Overall length in mm	250	140	250
Width in mm	25	25	36
Thickness in mm	2.88	5.28	2.88
Tab length* in mm	50	65	–
Free test length in mm	150	10	250
Gage length** in mm	150	–	–
Gage width** in mm	21	–	–

section. In the case of the impacted samples, the width was increased to 36 mm so that the damage of the impact does not reach the edges of the samples and growth of the damage can be determined in the further investigations. Suppose the impact already reaches the edge of the specimen. In that case, there will be interactions between the edge of the sample and the impact damage, which would not correspond to the component's structural behaviour. The fatigue samples, which are tested under compression-compression, correspond to the geometrical dimensions of the samples of the static compressive tests, except that the thickness has been reduced to 2.88mm (see Table 2). After sawing, the edges of the sample were finally grounded with abrasive paper (grid size 600 and 1200) to reduce edge effects caused by preparation steps before. The used standards and sample dimensions are summarized in Table 2.

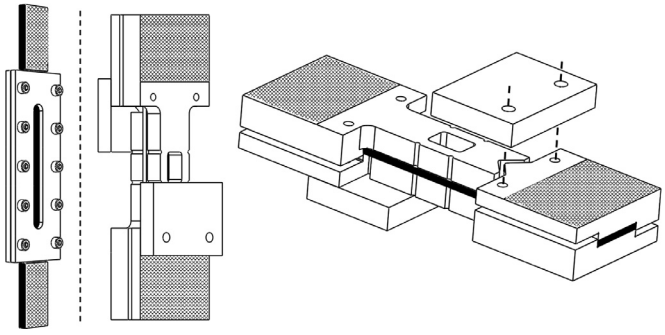

Fig. 1. Buckling supports for fatigue tests.

2.2. Experimental methods

The static tensile tests were carried out in accordance with ASTM D D3039-00 [40]. The clamping pressure of the servo-hydraulic clamping jaws amounted 140bar. The tests were performed on a ZwickRoell universal testing machine Z100 and strains were recorded using MultiXtens Extensometer from ZwickRoell. In the case of the thickest layer thickness (360 gsm), the crosshead displacement had to be used for the strain measurement, due to early delamination of the outer layers. The compression tests were carried out in accordance with ASTM D 6641-16 [41] performed using a ZwickRoell Z400 universal testing machine. IMA Dresden developed the used clamping system (HCCF) for compression tests of fibre reinforced composites at high compressive loads. The hydraulic pressure for the clamping jaws was 80bar. Vishay Precision Group (USA) strain gauges with a resistance of 350 Ω measured the strains. The fatigue tests were performed on servo-hydraulic testing machines from Instron. Three different load conditions were tested to investigate possible influences of the layer thickness on the failure behaviour. A load ratio of R = 0.1 was chosen for tensile-tensile tests. The samples were tested on an Instron 8800H2470 under stress control mode at 5Hz with a maximum force of 100 kN and servo-hydraulic clamps. The clamping pressure was 80bar. The displacement of the cylinder recorded the strains of the specimens. When a sample did not fail after being subjected to (10^6 cycles), the test machine stopped.

A load ratio of R=0.5 was chosen for the tension-compression tests. The tensile loads are twice as high as the compressive loads. Assuming that fibre composite materials are generally designed for tensile loads and therefore account for the main portion of operational stresses, therefore a load ratio of R=0.5 is an application-based approach. The hydraulic universal testing machine for tension-compression tests was the Instron 8800H2470 under stress control mode at 5Hz with a maximum force of 100kN and the Instron 8802L2741 under stress control mode at 3Hz with a maximum force of 250kN. In both cases, servo-hydraulic jaws with a clamping pressure of 80bar clamped the specimens. Due to the applied compressive forces and specimen geometry, two different buckling supports are utilised (see Fig. 1). For thicker layers, the buckling device supports the test length between the tabs (Fig. 1, left). However, this was not possible with the thinnest layer thickness (30 gsm), because a buckling failure occurred in the support-free section between the clamping of the specimen and the buckling support. The new buckling support was designed after the Open Hole Compression (ASTM D 6484-04 [42]) test jig, with the difference that the load is introduced via shear forces. The buckling support has the advantage that the sample is supported along its entire length, thus preventing local buckling, and transverse contraction is not hindered. The same setup is used for the fatigue after impact tests with a load ratio of R=0.5.

The R-ratio of the compression-compression tests was chosen to be R=10. Due to the gauge length of 10 mm and the thickness of 2.88mm, no buckling support was necessary. The specimens were tested on the Instron 8800H2470 servo-hydraulic testing machine under stress control mode at 5Hz with a maximum force of 100kN and servo-hydraulic jaws at 120bar clamping pressure. The displacement of the cylinder determined the strain.

The impact testing machine was the FW Primus 1700 Plus from Coesfeld Materialtest, Germany. The impacts were applied by using an

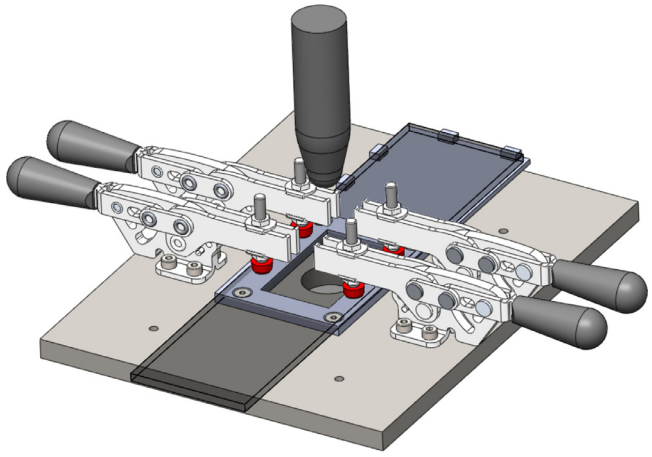

Fig. 2. Clamping device for impact tests.

Table 3
Number of tested samples for each ply thickness and load case.

	Fibre areal weight in gsm				
	30	60	120	240	360
Tension	7	6	6	6	5
Compression	6	6	6	6	5
Fatigue R=0.1	20	10	10	–	9
Fatigue R=0.5	19	7	7	–	14
Fatigue R=10	10	13	10	–	7
FAI R=0.5	8	6	8	–	5

impacter with a diameter of 16 ±0.1mm, a hardness between 60 and 62HCR and weight of 5.34kg and a rebound apparatus prevented multiple impacts. The maximum impact energy was 8J. Preliminary tests have shown that impact energy of over 8J leads to delamination up to the edges of the sample and due to the impact system, lower energies were not possible. The clamping design of the support structure was based on the ASTM D7136-05 (Standard test method for measuring the damage resistance of a fibre-reinforced polymer matrix composite to a drop-weight impact event [43]) with cut-out dimensions of 27 × 60mm. The ratio of length and width is identical to the standard. Four rubber tips restrain the specimen during impact with a minimum holding capacity of 1100N. Mechanical end stops aligned the samples (see Fig. 2).

To analyse the occurring damage and possible growth, samples were stopped at 0, $5 \cdot 10^4$, $3 \cdot 10^5$ and $8 \cdot 10^5$ cycles and examined using computed tomography. The system used is a CT-Alpha device from Procon X-Ray, Germany. The measurements of the damaged sample regions were taken in axial and helical mode with an x-ray tube voltage of 65kV and a voxel size of 27.3 and 24.3μ m, respectively. The helical scan mode was applied to samples (for example 360 gsm) with a large estimated damage area to capture the complete damaged area while maintaining a small voxel size. The visualization of the volume data, i.e. evaluation and graphical representation of impact damage as well as the damage progression according to the respective load cycles was done with the Volume Graphics VGSTUDIO MAX 3.3 software.

3. Results and discussion

3.1. Tensile tests

The results of the static tensile tests are shown in Fig. 3. At least five samples were tested for each configuration. Table 3 shows the number of tested samples for each ply thickness and load case. The tensile strength increases significantly with decreasing layer thickness in the range between 360 gsm and 60 gsm. Even lower layer thicknesses, 30 gsm, show no further improvement compared to the 60 gsm samples. However, the strength doubles between the 360 gsm and 30 gsm or 60 gsm samples. In case of the 360 gsm samples, the outer ±45° and 90° layers fully delaminate at low strains, and therefore the load is mainly transferred by the middle 0° layers, which significantly reduce the strength. This behaviour is not observed at lower layer thicknesses. Fig. 3 shows on the right-hand side the stress-strain curves of the tensile tests. It can be seen that all configurations have the same stiffness at low strains, as this is mainly dependent on the fibres and their orientation. However, with increasing load, initial damage occurs, and a decrease in stiffness is recorded for thicker layers. Further, samples with thinner layers (30 and 60 gsm) do not show any damage until final failure, and therefore no decrease in stiffness can be determined. The 30 and 60 gsm specimens' fracture patterns show a brittle failure behaviour and exhibit no or almost no delaminations. In both cases, the energy at the crack tip as well as the interlaminar shear stresses are too low to initiate delamination. As a result, the failure behaviour is fibre-dominated in both cases, and thus no differences between the layer thicknesses can be observed. Although theoretically the strength of the 90° layers should increase exponentially with decreasing layer thickness due to the in situ effect, the influence is too small compared to the influence of the fibres in 0° to measure a significant change. The layer thickness at which delamination is completely suppressed depends on the materials used and their properties, such as the toughness of the matrix. Detailed investigations on this can be found in a study by Cugnoni et al. [44]. With increasing layer thickness, a more delamination-dominated failure behaviour occurs. As a result, it can be concluded that under static tensile load, a layer thickness of 60 gsm in combination with the fibre and resin system used in this study already shows the maximum achievable strength and a reduction of the layer thickness does not offer any further advantage to the mechanical properties investigated. The freedom of design due to the higher number of layers is still an advantage.

3.2. Compressive tests

The results of the compressive tests show a significant increase in strength with decreasing layer thickness from 360 gsm to 30 gsm. Each configuration was tested with a minimum of five samples (see Table 3). Diagrams in Fig. 4 show the compressive strengths and stress-strain curves. The curve characteristics show that progressive failure occurs with low layer thicknesses. Initial damage or first local buckling does not lead to final failure as for thicker layers under compressive load. Due to the high amount of fibres and the distribution of the 0° layers, the samples have a relatively high bending stiffness after first damage, which leads to a decrease in stiffness but not to a final failure. A further advantage regarding the behaviour under compressive load is in the laminate quality. As already investigated in other studies, laminate quality improves with thinner layer thicknesses [18,23]. Fibre spreading results in a more homogeneous fibre arrangement and smaller resin-rich regions. In the case of thicker layers, initial damage already leads to final failure, as the bending stiffness is significantly reduced. Defects and resin-rich regions act as initiators for possible initial damage.

3.3. Fatigue tests

3.3.1. Tension – Tension

The results of the tension-tension tests are shown in Fig. 5. The diagram on the left-hand side represents the S-N curve (Wöhler curve), here the amplitude stress is plotted against the number of cycles to failure on a logarithmic scale. Each configuration was tested with at least nine samples. Due to the non-standard failure of the 30 gsm samples at higher stresses, 20 samples were tested in this case. The non-filled points represent samples which have reached the run-out criterion of 10^6 cycles. Solid lines show the calculated failure probability that 50% of the specimens will fail at this number of cycles at a specific stress amplitude.

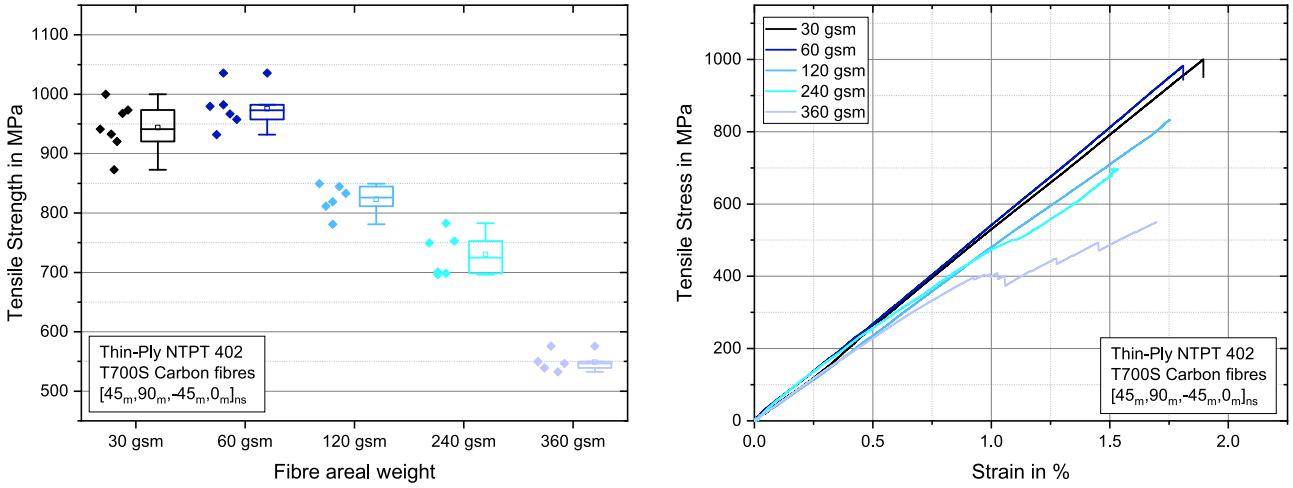

Fig. 3. Tensile strength (left) and tensile stress-strain curves (right) depending on the layer thickness.

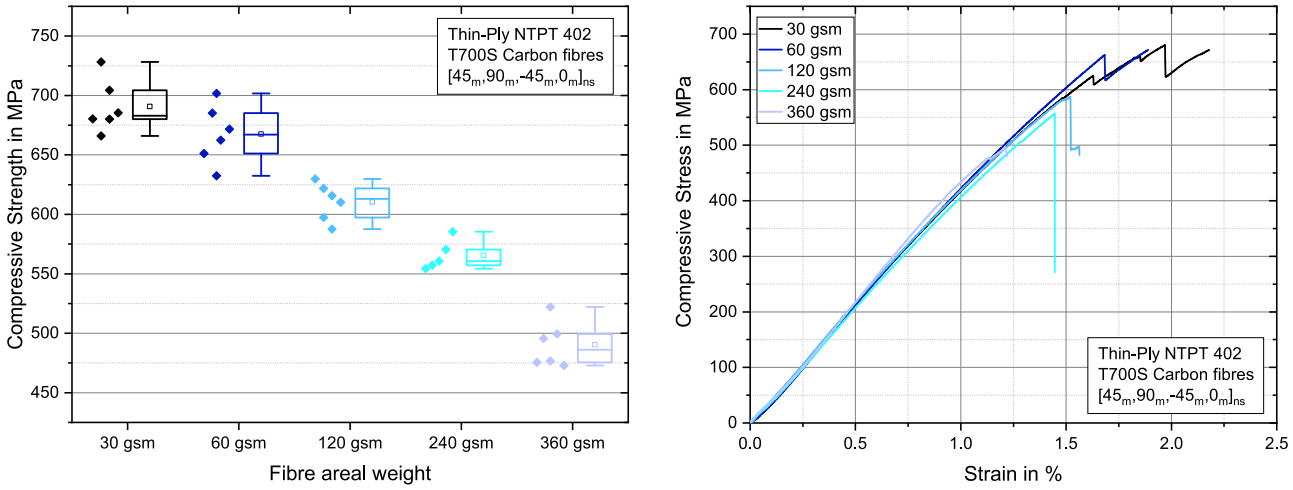

Fig. 4. Compressive strength (left) and compressive stress-strain curves (right) depending on the layer thickness.

The 50% probability of failure of the 360 gsm samples is significantly lower than that of the other samples, although the curve is relatively flat. Due to the high layer thickness, all 0° layers are in the middle of the lay-up. The outer layers fully delaminate at low numbers of cycles, resulting in a type of unidirectional sample. Still, the resulting unidirectional load-bearing layers results in a flat S-N curve since the fatigue properties are essentially dependent on the 0° carbon fibres. The behaviour is also apparent in the stiffness degradation curve. On the right-hand side is the relative stiffness, which is the quotient of the stiffness at cycle n and the initial stiffness of the first cycle. In this study, stiffness is defined as the slope of the tangent of the stress-strain curve (hysteresis) at 5% and 50% of the maximum stress of each hysteresis recorded. The typical shape of a S-N curve consists of three phases. An early decrease in stiffness combined with initial damage such as inter-fibre fractures, a relatively constant plateau on which the damage grows, and a slight but continuous decrease in stiffness occurs, and finally a considerable reduction in stiffness and ultimate failure. In the case of the 360 gsm samples, a fourth phase has occurred, a plateau with constant stiffness. In this phase, all outer layers are already delaminated, and only the 0° layers in the middle of the specimens are loaded.

There is a significant improvement in the fatigue stress of the 60 gsm and 120 gsm compared to the 360 gsm samples. The 50% probabilities of failure are shifted to higher stress amplitudes, and both S-N curves are steeper than the curve of the 360 gsm samples, where the 60 gsm specimens can handle even higher stresses. Both layer thicknesses have a similar slope of the S-N curve and are equally sensitive to failure behaviour. However, the relative stiffness show also differences between them. The curve of the 120 gsm samples have a fourth phase, as do the 360 gsm samples, which in turn is due to the relatively thick sub-laminate in the middle of the lay-up. The 60 gsm samples do not show this fourth phase any more. The second decrease in stiffness leads to final failure; it can also be seen in the fracture patterns. The 120 gsm samples show a failure behaviour dominated by delaminations, whereas the 60 gsm samples fail relatively brittle, and only a few delaminations are visible. As the static tensile tests have already shown, the formation of delaminations is suppressed, and brittle failure occurs. The failure behaviour under tensile-tensile load is similar to the failure behaviour under static tensile load.

As described in the section materials and specimen preparation, the 30 gsm samples had to be tested with the shape of a dogbone sample. Without this geometry change, all specimens fail in the load introduction area and therefore not conforming to the standard. Due to the brittle properties of the material and the suppression of damage, high local stress concentrations occur in the load introduction area, which leads to premature failure. Amacher et al. investigated fatigue open hole tensile (OHT) tests and observed that at higher stresses, thinner layer thicknesses lead to early failure because no stresses can be dissipated or diverted due to pre-damage in the area of the stress concentration. Below a certain stress amplitude, no damage occurs, and the fatigue properties improve significantly [18].

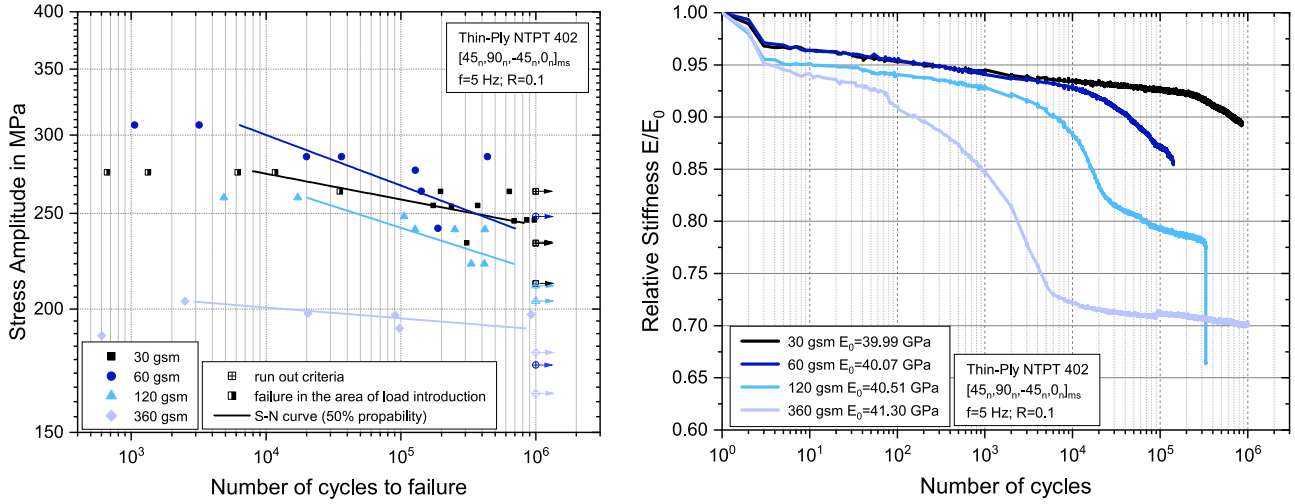

Fig. 5. S-N curves of the fatigue results with a load ratio of R=0.1 (left) and relative reduction of the specimen stiffness (right).

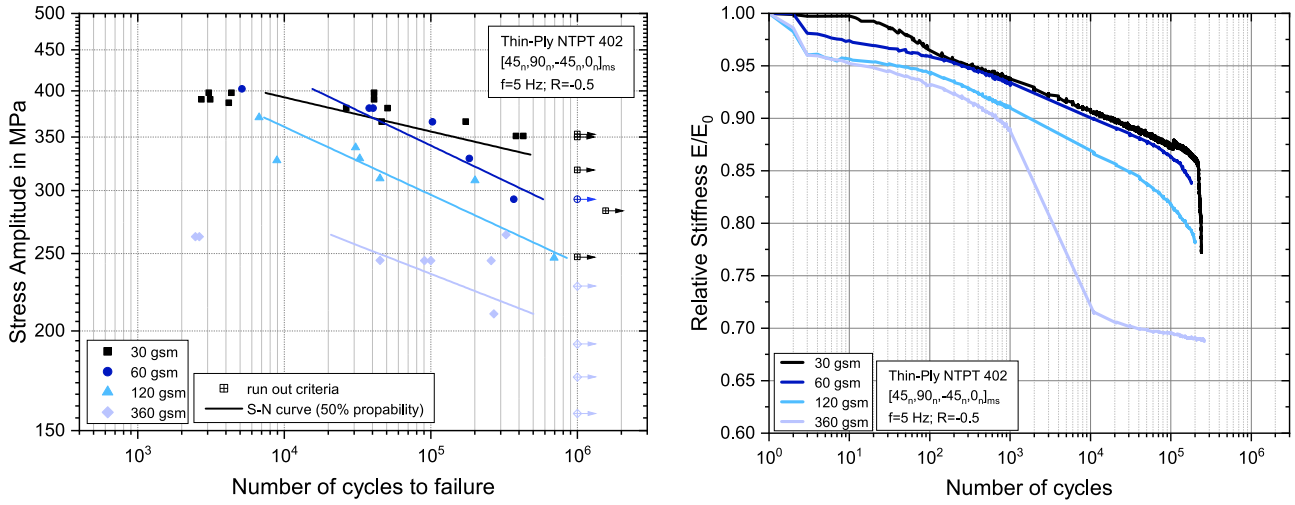

Fig. 6. S-N curves of the fatigue results with a load ratio of R=-0.5 (left) and relative reduction of the specimen stiffness (right).

Despite the change in specimen geometry, the specimens failed near the load introduction area at high stresses (see Fig. 5, open-symbols). The fracture patterns of the tested specimens in this study show an increased failure in the area of load introduction for the samples with high stresses (half-filled squares) despite the sample geometry. At lower stresses, the specimens fail according to the standard within the smaller cross-section area. The stress concentrations in the load introduction area are below the apparently critical stress. In the development of the stiffness decrease, brittle material behaviour can be recognized. The knowledge of the suppression of pre-damage and the results of Amacher et al. regarding stress concentrations, suggests that thin-layer laminates have improved fatigue properties at low stresses and high numbers of cycles. To investigate the fatigue behaviour under higher stresses, the load introduction area or the sample geometry must be further modified so that the load introduction is not the critical area.

3.3.2. Tension - Compression

The fatigue results with a load ratio of R=-0.5 (Fig. 6) show similar behaviour to the tension-tension tests. At least seven specimens were tested for each configuration. However, as the 30 gsm specimens failed in a non-standard way at higher stresses, 20 specimens were tested here. In general, the fatigue properties improve with decreasing layer thickness. In the case of the 60, 120 and 360 gsm samples, no change in the slope of the S-N curves is apparent. The curves are shifted in height. Only the S-N curve of the 30 gsm samples shows a lower gradient as under tension-tension. Here the intersection of the 30 gsm and the 60 gsm S-N curve is at about 40,100 cycles and a stress level of 370MPa. Also, in this case, stress concentrations at thin layer thicknesses will lead to premature failure at higher stresses in the load introduction area. In the tensile-tensile tests, specimens failed at amplitude stress of about 258MPa near the tabs, which corresponds to a maximum stress of 572MPa. The tensile-compressive samples fail in the area of the tabs at amplitude stress of about 381MPa, which corresponds to a maximum stress of 508MPa. However, the two stresses are not directly comparable since the stress of the tensile-tensile specimens refers to a smaller cross-section area due to the specimen design of a dogbone. However, the tabs of the samples have the same geometric dimensions and, when the force per mm of specimen thickness is calculated, the critical load is 12.03kN/mm for the tensile-tensile specimens and 12.70kN/mm for the tensile-compressive specimens. Thus the same problems arise under tensile-compressive load as under tensile-tensile load. Nevertheless, thinner layers display superior fatigue behaviour at higher load cycles, as they occur in industrial applications.

The right diagram of Fig. 6 shows that the stiffness decreases over the number of cycles. The curves do not show a typical horizontal plateau as under tension-tension, but a region with a constant stiffness decrease. The stiffness degradation of the 30, 60 and 120 gsm samples looks very

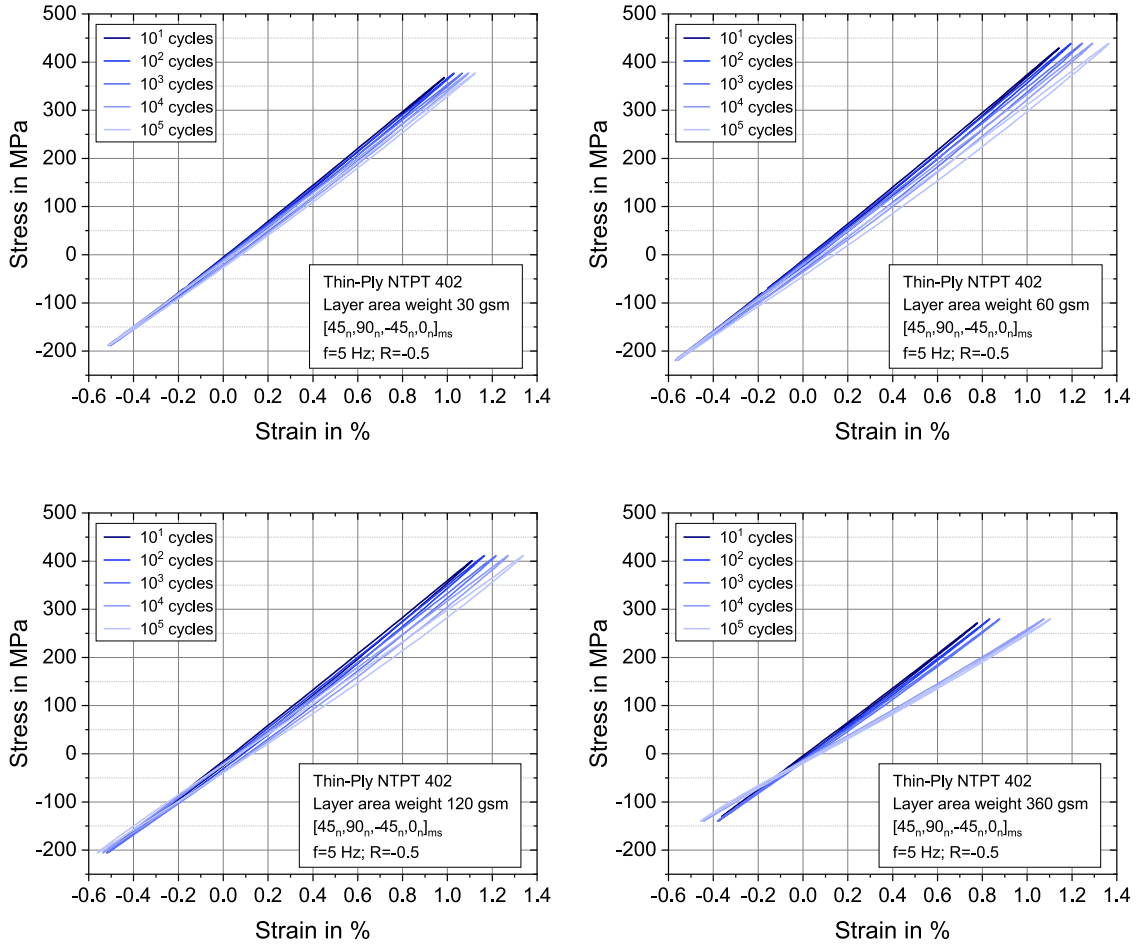

Fig. 7. Hysteresis of different layer thicknesses (upper left: 30 gsm, upper right: 60 gsm, lower left: 120 gsm and lower right: 360 gsm) at 10^1, 10^2, 10^3, 10^4 and 10^5 cycles.

similar. Noticeable is the strong decrease of the 360 gsm sample in the range between 1000 and 10,000 cycles. To describe this reduction in stiffness in more detail, Fig. 7 shows the hysteresis of the samples. The diagrams show the hystereses of 10^1, 10^2, 10^3, 10^4 and 10^5 cycles. The hysteresis of a 30 gsm sample is in the upper left, of a 60 gsm sample in the upper right, of a 120 gsm sample in the lower left and a 360 gsm sample in the lower right corner. With increasing layer thickness, the angular offset concerning the first cycles increases and the area of the hysteresis (energy per cycle) decreases with decreasing layer thickness. A flatter hysteresis exhibits a lower stiffness due to damage like inter-fibre fractures and delaminations. In the case of the 360 gsm samples (bottom right), the first 1000 hysteresis are similarly superimposed, but the angle of the hysteresis at higher numbers of cycles change strongly. This is due to the formation of delaminations between the outer layers and the 0° layers in the middle of the samples. The small opening of the hysteresis of the 360 gsm sample at a high number of cycles, indicates that only the 0° layers are loaded, and no energy is dissipated due to open and close of inter-fibre fractures or delaminations. It can be seen that the deviation between the hysteresis is smaller with lower layer thicknesses, which indicates a constant material behaviour independent of the number of cycles. As in the static, a brittle material behaviour of the thin layer thicknesses can be seen.

3.3.3. Compression – Compression

Fig. 8 shows the S-N curves of the fatigue tests under compressive-compressive load (R=10). For each configuration, at least seven samples were tested. The results demonstrate an improvement of the fatigue properties with decreasing layer thickness. Due to the test setup and the

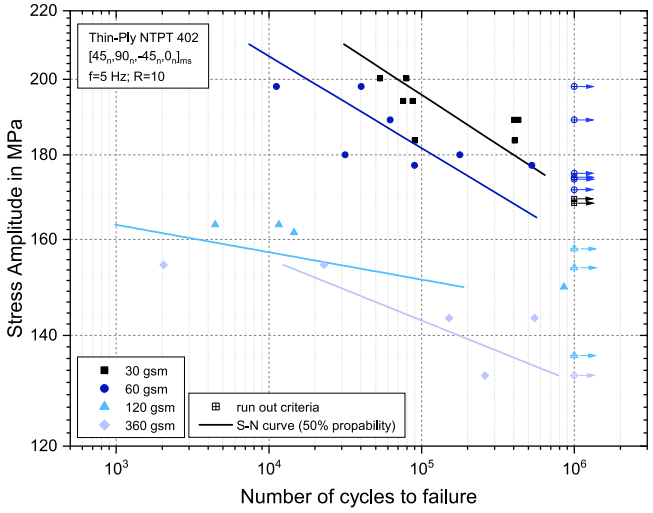

Fig. 8. S-N curves of the fatigue results with a load ratio of R=10.

failure behaviour of fibre composites under compression, there is a significant scatter within the results. Still, the gradient of the S-N curves shows differences. The slopes of the 30 and 60 gsm samples are much steeper. Fracture patterns of tested specimens in Fig. 9 show a changing failure mechanism, as can also be found under static compressive loading of quasi-isotropic samples. The micrographs represent fracture

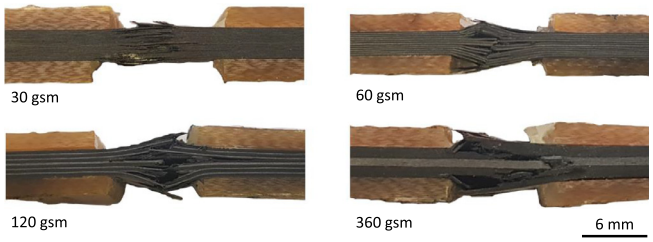

Fig. 9. Fracture pattern of the fatigue tested samples with a load Ratio of R=10 (compression-compression).

patterns of four specimens that have been loaded about a half a million cycles to failure. In the case of the 360 gsm specimens, the outer layers delaminated at a low number of cycles. The failure behaviour is a combination of through-thickness (0° layer), and brooming [45]. Due to the absence of supporting layers, the middle 0° layers started to bend, and the final failure occurred. The 60 gsm and 120 gsm samples show a similar failure pattern. In both cases, brooming occurs, and delaminations and sub-laminates have formed. In the case of the 120 gsm samples, the sub-laminates usually consist of four layers with one 0° layer on the outside, so that the sub-laminates are fragile against buckling. In contrast, the sub-laminates of the 60 gsm samples consist of more than four layers and 0° layers are not only at the outside of the sub-laminates. These layers significantly increase the bending stiffness of the sub-laminates and improve the mechanical properties under compressive load. Furthermore, the materials in this study, as well as previous studies by other laboratories ([16–18]), show that the quality of the laminates or prepregs improves with decreasing layer thickness. The higher material qualities have a positive effect on the behaviour under compression. The fracture pattern of the 30 gsm sample differs from the other samples. Delamination occurs in a small area, and the fracture patterns show no buckling of the outer layers or sub-laminates. The fracture pattern shows a longitudinal splitting, and the layers slide together more like a comb. The stop criterion of the fatigue stress-controlled tests was set with a maximum displacement. The 30 gsm samples show a residual compressive strength even after stopping the tests. By pushing the layers or sub-laminates together, relatively high bending stiffness is still present. However, due to the displacement of the upper and lower part of the specimen, the test had to be stopped. For industrial applications, the failure behaviour implies a high safety factor concerning the use of Thin-Ply under cyclic compressive load. Despite damage, there is a relatively high residual stiffness and strength.

3.3.4. Constant-life diagram

The constant-life diagram in Fig. 10 summarized the fatigue results obtained. The mean stress is plotted on the abscissa and the amplitude stress on the ordinate. Each point represents the ratio between mean stress and amplitude stress as a function of the load ratio at $5 \cdot 10^5$ cycles. The theoretical interpolations between the measured values are calculated according to the piecewise linear interpolation of Philippidis et al. [34]. A reduction of the layer thickness results in an improvement of the fatigue properties and higher number of load cycles can be tolerated at the same stress level. Only tensile-tensile loading (R=0.1), the 30 gsm achieved no significant improvement compared to the 60 gsm samples. However, as previously presented, the reduced layer thicknesses under high loads in the tensile area of the hysteresis resulted in damage in the area of load introduction. At higher numbers of load cycles, the thin layer thicknesses within this study show advantages. It is also noticeable that especially under tensile-compressive loading (R=0.5) the thin layer thicknesses have a significant improvement. Due to the damage suppression, no pre-damage initiates under tension load, leading to a significant stiffness reduction under compressive load. Especially in the alternating load range, the advantages of thin layer thicknesses become apparent.

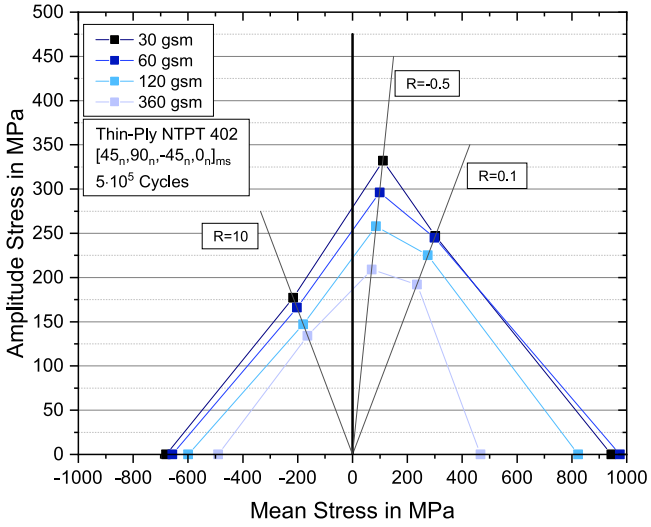

Fig. 10. Constant-life diagram for n = $5 \cdot 10^5$ cycles, piecewise linear interpolation.

Furthermore, even if the static tensile and compressive tests show only minor improvements of the 30 gsm compared to the 60 gsm specimen, the improvement is higher under fatigue loading (R=0.5). The results show that the load case should be taken into account if the performance of fibre composites is to be improved by reducing the layer thickness. In areas with alternating loads, it is reasonable to use thinner layers. Nevertheless, the failure behaviour should be taken into account. In the case of tensile loads, brittle failure occurs, especially with thin layers, which is a disadvantage in practical applications. In the case of compressive loads, on the other hand, a progressive failure occurs with the thinner layers, which is to be evaluated positively under certain conditions. In summary, the results show that the use of thin layers can be useful. Still, it has to be considered carefully depending on the applied stresses and failure behaviour.

3.4. Fatigue after impact

3.4.1. Impact

Fig. 11 shows representative ultrasonic images and micrographs of the occurring impact damage. The ultrasonic images illustrate the defect depth of the damage. The ultrasound images illustrate the defect depth of the damage, and an approximation of the depth is visualized by different colours. If there are several damages on top of each other, only the uppermost damage could be detected. The ultrasonic images demonstrate that the extent of the damaged area and the damage pattern depends on the layer thickness. The 360 gsm samples show a typical failure behaviour for fibre reinforced composites. Inter-fibre fractures and delaminations are visible, which increase with the depth of the sample. Depending on the fibre orientation, the damage spread out in a different direction. Numerous studies have described the failure behaviour of fibre reinforced composite structures under impact load so that reference will be made to them here [4,46]. With decreasing layer thickness, the failure pattern of the samples changes. The number and length of inter-fibre fractures decrease until they are entirely suppressed in the case of the 30 gsm sample, as has also been shown by Arteiro et al. and Saito et al. [20,27]. The 60 gsm samples show fewer inter-fibre fractures but many delaminations. Sub-laminates are formed, which have a thickness of four layers, 240μ m. The high number of delaminations is untypical for CAI samples (ASTM D7137-05 [47]) with thin layers. However, the untypical fracture pattern results from the smaller clamping device used in this study.

In contrast to the larger CAI specimens, less material can absorb energy and locally the damage is increased. Due to the small deformations

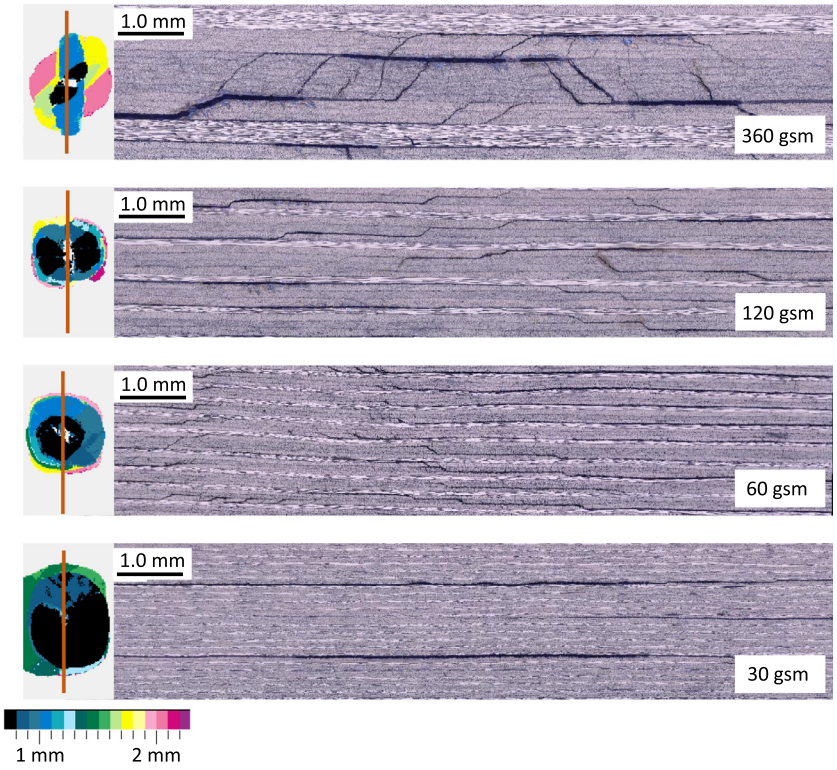

Fig. 11. Ultrasonic C-Scan images (left) and micrographs (right) of the impact for a potential impact energy of 8J, from top to bottom: 360 gsm, 120 gsm, 60 gsm and 30 gsm.

and the suppression of inter-fibre fractures, less energy can be dissipated elastically, and high shear stresses are applied, which initiate delaminations. The shape of the delaminations has changed from a peanut to a circular shape. In the case of the 30 gsm sample, three large circular delaminations occurred. The first delamination develops between the middle layers, the highest shear stress area, and two sub-laminates are formed. A further load increases the shear stresses within the two sub-laminates. If the shear stresses also exceed the critical stress in the sub-laminates between the new middle layers, further delaminations occur. The shear stresses between the other layers are not sufficient to initiate further delaminations as with the 60 gsm samples. About 50% of the 30 gsm samples show this failure pattern. The other 50% show a similar failure pattern to the 60 gsm samples. It appears that the test setup is at a tipping point between the two failure modes. It was not possible to increase the energy because higher energies caused fibre breaks on the backside of the specimen. Lower energies were not possible because of the test setup and machine used.

3.4.2. Fatigue after impact

Fig. 12 shows the S-N curves of the pre-damaged samples. A total of 27 samples were tested. 8 samples each with a fibre areal weight of 30 and 120 gsm, 6 with 60 gsm and 5 with 360 gsm (see Table 3). The solid lines correspond to the S-N curves of the pre-damaged samples and the dashed lines to the S-N curves of the samples without impact damage. As expected, the lifetime of the pre-damaged samples is shorter than that of the undamaged samples. However, the difference between the pre-damaged and non-damaged specimens varies between the layer thicknesses. Considered at 10^5 cycles, the 60 gsm and 360 gsm samples show the highest decrease of fatigue stress with 31.9% and 28.1% respectively.

As seen in the micrographs, the samples with a layer thickness of 360 gsm show large delaminations and matrix cracks (see Fig. 11). The growth of damage with an increasing number of load cycles reduces the fatigue strength. A computed tomography system examined the pre-damaged samples after a certain number of cycles and compared the

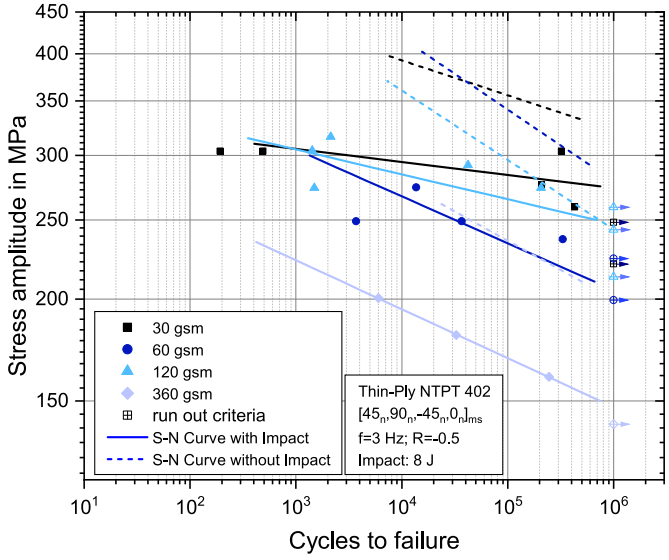

Fig. 12. S-N curves of the fatigue after impact results with a load ratio of R=-0.5 and an potential impact energy of 8J.

damage patterns. The samples were stopped and analysed after 0, $5 \cdot 10^4$, $3 \cdot 10^5$ and $8 \cdot 10^5$ cycles. Fig. 13 presents representative tomography images of the 30 gsm and 360 gsm pre-damaged samples after loading. The damage patterns of the 360 gsm specimen show large, orientation-driven delaminations. The damaged area increases significantly with the increasing number of cycles. The delaminations reach the edge of the sample after only $5 \cdot 10^4$ cycles, and cracks are visible on the top surface after $3 \cdot 10^5$ cycles. From the recorded data, sectional images of the respective samples were made, which show the current state of damage perpendicular to the load, see Fig. 14. The damage of the 360 gsm

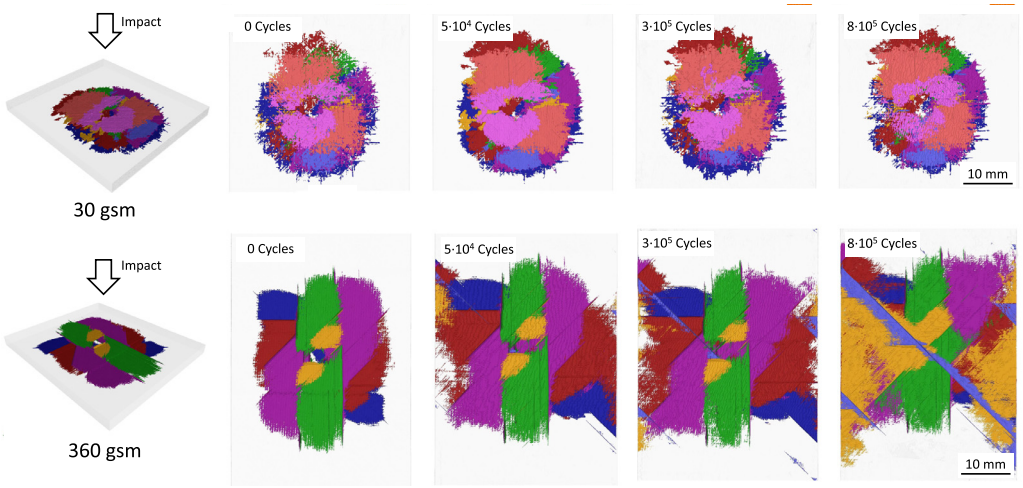

Fig. 13. Computed tomography images of the impact damage of the 30 gsm (top) and the 360 gsm sample (bottom). The left two images show the initial state after the impact, the three right images show the damage pattern after cyclic loading of $5 \cdot 10^4$, $3 \cdot 10^5$ and $8 \cdot 10^5$ cycles. Colours are chosen arbitrary and indicate layers of damage at different depths.

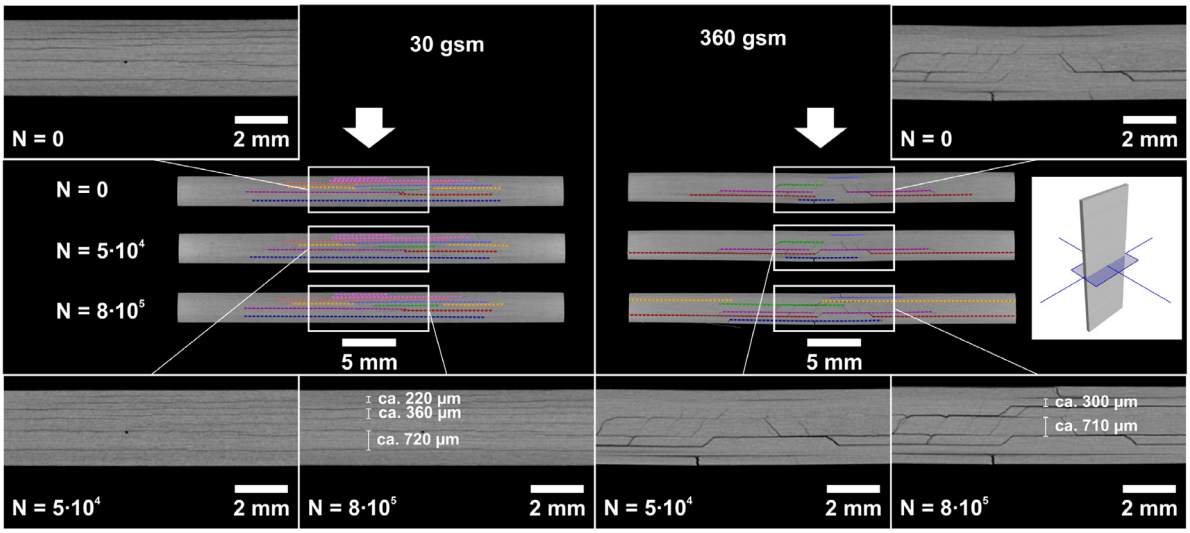

Fig. 14. Cross sections of the impacted specimens (left 30 gsm and right 360 gsm) after 0, $5 \cdot 10^4$ and $8 \cdot 10^5$ cycles. Colours are chosen arbitrary and indicate layers of damage at different depths.

sample growth perpendicular to the tensile direction. Due to the fatigue loading, further inter-fibre fractures have formed, which lead to delaminations and existing delaminations grow due to high interlaminar shear stresses. Slight buckling of the specimen, as caused by the impact (asymmetric damage), increases the stresses within the crack tip of delamination, which supports damage growth. The micrograph of the 60 gsm sample also shows a high number of delaminations. Each sub-laminate consists of four layers and thus has a thickness of about 240μ m. The individual delaminations are arranged circularly around the impact (see Fig. 11). This geometric arrangement weakens the material in all spatial directions and favours a buckling of the sample or the layers, resulting in premature failure. Additionally, the individual sub-laminates have a low bending stiffness; the respective 0° layer is located on the outside at the sub-laminates and is not supported against buckling.

As already described in the previous part, the 30 gsm samples show two different failure patterns. Some samples show few but very large delaminations (Fig. 11), and other samples show more and smaller delaminations like the 60 gsm samples. The computed tomography measurements allow a non-destructively 3-dimensional visualisation of the damage pattern. Fig. 14 shows cross-sections of the impacts from Fig. 13 perpendicular to the loading direction. The delaminations are highlighted, and the colours are chosen arbitrary and indicate damage at different depths. In addition to the cross-sections, detailed images from the respective impact area are shown, and the thicknesses of the sub-laminates are measured. The CT-cross-sections reveal that the thinnest sub-laminates are approx. 220μ m thick and have at least eight CFRP layers. However, thicker sub-laminates are also visible up to 720μ m. Due to the higher number of CFRP layers and the support of the inner 0° layers against buckling, the sub-laminates have a higher bending stiffness than the sub-laminates of the 60 gsm samples. As with the 60 gsm samples, a circular arrangement of the delaminations can be found, which would indicate a large reduction in fatigue properties. However, the specimens lifetime decreased by only 20.3%. The tomography cross-sections demonstrate that with an increasing number of cycles, the damage does not grow any further and a static state of damage is achieved. The laminate exhibit no matrix cracks, and the formation of delaminations is suppressed. The interlaminar shear stresses are not sufficient for the growth of delaminations. Due to the large number of layers and the associated high number of interfaces, the interlaminar shear stresses are lower between the layers. The cross-sections of the tomography scans of

the 360 gsm samples show a damage progression (green and red delamination) and also new damages such as inter-fibre fractures and delaminations (yellow delaminations) with an increasing number of cycles. As a result, the lifetime is reduced.

The 120 gsm samples exhibit the smallest reduction in fatigue performance. Contrary to this trend, the micrographs in Fig. 11 show inter-fibre fractures and delaminations. Concerning the residual stiffness of the sub-laminates, the delaminations are between the 0° and 45° layers. The differences between the 120 gsm and samples with thinner layers (30 and 60 gsm) can be seen in the ultrasound images in Fig. 11. The delaminations are not circular but have the shape of a peanut. Thus, although larger delaminations are present, they spread preferentially in the direction of the fibre orientation in the layer. The delamination areas are small in transverse direction to the preferred delamination orientation, leading to a high local residual stiffness.

4. Conclusion

The fatigue behaviour of undamaged and impacted samples of quasi-isotropic high-performance composites was investigated in this study. Static tensile and compressive tests, as well as fatigue tests under different load ratios and layer thicknesses were carried out, and a prediction of fatigue behaviour is given by a linear interpolation method. The undamaged test results show that the static and fatigue strength increase with decreasing layer thickness and depends on the load ratio. In the tensile-compressive load range (R=-0.5) in particular, significant improvements can be achieved using thin layers. The formation of inter-fibre fractures and delaminations are suppressed under tensile load, leading to lower damage growth under compressive load and higher lifetimes. The 30 gsm specimens exhibit a 58.94% improvement in lifetime at a maximum stress of 50% of the tensile strength compared to the 60 gsm samples. The reduction of layer thickness is leading to a larger loading space.

Although the impact damages of the 30 gsm samples have significantly larger projected delamination areas, they have less influence on the fatigue behaviour of the samples. Computed tomography images show that the damage does not spread within the Thin-Ply layers. In the case of the 360 gsm samples, the delaminations already grow at low numbers of cycles and reach the edge of the sample after $5 \cdot 10^4$ cycles and lead to final failure. In addition to delamination growth, the shape of delaminations and layer structure of the sub-laminates also have a significant influence on the lifetime. Local higher bending stiffness, as in the case of peanut-shaped delaminations or sub-laminates with internal 0° layers, lead to an improvement in lifetime.

From the results obtained from this study, it can be concluded that fatigue behaviour of undamaged and impacted samples is superior with thinner layer thicknesses. Still, for industrial applications, the trade-off between performance and costs has to be done, i.e. the suitable layer thickness depends on load ratio and effort of production.

Declaration of Competing Interest

The authors declare that they have no known competing financial interests or personal relationships that could have appeared to influence the work reported in this paper.

Supplementary material

Supplementary material associated with this article can be found, in the online version, at 10.1016/j.jcomc.2021.100139

References

[1] M. Mitrovic, Effect of loading parameters on the fatigue behavior of impact damaged composite laminates, Compos. Sci. Technol. 59 (14) (1999) 2059–2078, doi:10.1016/S0266-3538(99)00061-5.
[2] H. Schmutzler, M. Alder, N. Kosmann, H. Wittich, K. Schulte, Degradation monitoring of impact damaged carbon fibre reinforced polymers under fatigue loading with pulse phase thermography, Compos. Part B 59 (2014) 221–229, doi:10.1016/j.compositesb.2013.12.010.
[3] N. Kosmann, B.T. Riecken, H. Schmutzler, J.B. Knoll, K. Schulte, B. Fiedler, Evaluation of a critical impact energy in GFRP under fatigue loading, Compos. Sci. Technol. 102 (2014) 28–34, doi:10.1016/j.compscitech.2014.07.010.
[4] W.J. Cantwell, J. Morton, The impact resistance of composite materials – a review, Composites 22 (1991) 347–362.
[5] M. Capriotti, H.E. Kim, F.L. Di Scalea, H. Kim, Detection of major impact damage to composite aerospace structures by ultrasonic guided waves and statistical signal processing, Procedia Eng. 199 (2017) 1550–1555, doi:10.1016/j.proeng.2017.09.505.
[6] C. Garnier, M.-L. Pastor, F. Eyma, B. Lorrain, The detection of aeronautical defects in situ on composite structures using non destructive testing, Compos. Struct. 93 (5) (2011) 1328–1336, doi:10.1016/j.compstruct.2010.10.017.
[7] M.A. Omar, Y. Zhou, A quantitative review of three flash thermography processing routines, Infrared Phys. Technol. 51 (4) (2008) 300–306, doi:10.1016/j.infrared.2007.09.006.
[8] M. Alemi-Ardakani, A.S. Milani, S. Yannacopoulos, L. Bichler, D. Trudel-Boucher, G. Shokouhi, H. Borazghi, Microtomographic analysis of impact damage in FRP-composite laminates: a comparative study, Adv. Mater. Sci. Eng. 2013 (2013) 1–10, doi:10.1155/2013/521860.
[9] W. Cantwell, P. Curtis, J. Morton, Post-impact fatigue performance of carbon fibre laminates with non-woven and mixed-woven layers, Composites 14 (3) (1983) 301–305, doi:10.1016/0010-4361(83)90020-4.
[10] T.K. O'Brien, Characterization of Delamination Onset and Growth in a Composite Laminate, NASA Technical Memorandum, 1981.
[11] S.L. Ogin, P.A. Smith, P. Beaumont, Matrix cracking and stiffness reduction during the fatigue of a (0/90)s GFRP laminate, Compos. Sci. Technol. 22 (1) (1985) 23–31, doi:10.1016/0266-3538(85)90088-0.
[12] R. Talreja, Stiffness properties of composite laminates with matrix cracking and interior delamination, Eng. Fract. Mech. 25 (5–6) (1986) 751–762, doi:10.1016/0013-7944(86)90038-X.
[13] N. Kosmann, J.M. Karsten, M. Schuett, K. Schulte, B. Fiedler, Determining the effect of voids in GFRP on the damage behaviour under compression loading using acoustic emission, Compos. Part B 70 (2015) 184–188, doi:10.1016/j.compositesb.2014.11.010.
[14] K. Senthilnathan, C.P. Hiremath, N.K. Naik, A. Guha, A. Tewari, Microstructural damage dependent stiffness prediction of unidirectional CFRP composite under cyclic loading, Compos. Part A 100 (2017) 118–127, doi:10.1016/j.compositesa.2017.05.010.
[15] R. Protz, N. Kosmann, D. Fritsch, P. Fey, W. Essig, K. Dietrich, M. Gude, P. Horst, M. Kreutzbruck, K. Schulte, G. Busse, W. Hufenbach, B. Fiedler, Influence of voids and impact damage on the fatigue behaviour of large scale composites, Materwiss Werksttech 47 (11) (2016) 1058–1071, doi:10.1002/mawe.201600631.
[16] K. Kawabe, S. Tomoda, T. Matsuo, A pneumatic process for spreading reinforcing fiber tow, in: 42nd International SAMPE Symposium, 1997, pp. 65–76.
[17] S. Sihn, R. Kim, K. Kawabe, S. Tsai, Experimental studies of thin-ply laminated composites, Compos. Sci. Technol. 67 (6) (2007) 996–1008, doi:10.1016/j.compscitech.2006.06.008.
[18] R. Amacher, J. Cugnoni, J. Botsis, L. Sorensen, W. Smith, C. Dransfeld, Thin ply composites: experimental characterization and modeling of size-effects, Compos. Sci. Technol. 101 (101) (2014) 121–132, doi:10.1016/j.compscitech.2014.06.027.
[19] A. Arteiro, G. Catalanotti, A.R. Melro, P. Linde, P.P. Camanho, Micro-mechanical analysis of the in situ effect in polymer composite laminates, Compos. Struct. 2014 (116) (2014) 827–840, doi:10.1016/j.compstruct.2014.06.014.
[20] A. Arteiro, C. Furtado, G. Catalanotti, P. Linde, P.P. Camanho, Thin-ply polymer composite materials: a review, Compos. Part A 132 (2020) 105777, doi:10.1016/j.compositesa.2020.105777.
[21] B. Kötter, K. Yamada, J. Körbelin, K. Kawabe, M. Nishikawa, M. Hojo, B. Fiedler, Steel foil reinforcement for high performance bearing strength in thin–ply composites, Compos. Part C 4 (2021) 100085, doi:10.1016/j.jcomc.2020.100085.
[22] B. Kötter, J. Karsten, J. Körbelin, B. Fiedler, CFRP thin-ply fibre metal laminates: influences of ply thickness and metal layers on open hole tension and compression properties, Materials (2020), doi:10.3390/ma13040910.
[23] T. Yokozeki, Y. Aoki, T. Ogasawara, Experimental characterization of strength and damage resistance properties of thin-ply carbon fiber/toughened epoxy laminates, Compos. Struct. 82 (3) (2008) 382–389, doi:10.1016/j.compstruct.2007.01.015.
[24] A. Arteiro, G. Catalanotti, J. Xavier, P.P. Camanho, Notched response of non-crimp fabric thin-ply laminates: analysis methods, Compos. Sci. Technol. 88 (2013) 165–171, doi:10.1016/j.compscitech.2013.09.003.
[25] P.P. Camanho, C.G. Dávila, S.T. Pinho, L. Iannucci, P. Robinson, Prediction of in situ strengths and matrix cracking in composites under transverse tension and in-plane shear, Compos. Part A 2006 (37) (2006) 165–176, doi:10.1016/j.compositesa.2005.04.023.
[26] M.J. Laffan, S.T. Pinho, P. Robinson, L. Iannucci, Measurement of the in situ ply fracture toughness associated with mode i fibre tensile failure in FRP. Part I: data reduction, Compos. Sci. Technol. 70 (4) (2010) 606–613, doi:10.1016/j.compscitech.2009.12.016.
[27] H. Saito, M. Morita, K. Kawabe, M. Kanesaki, H. Takeuchi, M. Tanaka, I. Kimpara, Effect of ply-thickness on impact damage morphology in CFRP laminates, J. Reinf. Plast. Compos. 30 (13) (2011) 1097–1106, doi:10.1177/0731684411416532.
[28] A.P. Vassilopoulos, B.D. Manshadi, T. Keller, Influence of the constant life diagram formulation on the fatigue life prediction of composite materials, Int. J. Fatigue 32 (4) (2010) 659–669, doi:10.1016/j.ijfatigue.2009.09.008.
[29] K. Yamaguchi, T. Hahn, The improved ply cracking resistance of thin-ply lami-

nates, in: International Conference on Composite Materials 15; Proceedings, 2005, pp. 1–10.
[30] B. Harris, A historical review of the fatigue behaviour of fibre-reinforced plastics, in: Fatigue in Composites, Elsevier, 2003, pp. 3–35, doi:10.1533/9781855738577.1.3.
[31] M. Kawai, M. Koizumi, Nonlinear constant fatigue life diagrams for carbon/epoxy laminates at room temperature, Compos. Part A 38 (11) (2007) 2342–2353, doi:10.1016/j.compositesa.2007.01.016.
[32] G. BOERSTRA, The multislope model: a new description for the fatigue strength of glass fibre reinforced plastic, Int. J. Fatigue 29 (8) (2007) 1571–1576, doi:10.1016/j.ijfatigue.2006.11.007.
[33] C. Kassapoglou, Fatigue life prediction of composite structures under constant amplitude loading, J. Compos. Mater. 41 (22) (2007) 2737–2754, doi:10.1177/0021998307078735.
[34] T.P. Philippidis, A.P. Vassilopoulos, Life prediction methodology for GFRP laminates under spectrum loading, Compos. Part A 35 (6) (2004) 657–666, doi:10.1016/j.compositesa.2004.02.009.
[35] M.H. Beheshty, B. Harris, T. Adam, An empirical fatigue-life model for high-performance fibre composites with and without impact damage, Compos. Part A 30 (8) (1999) 971–987, doi:10.1016/S1359-835X(99)00009-3.
[36] N. Tai, M. Yip, J. Lin, Effects of low-energy impact on the fatigue behavior of carbon/epoxy composites, Compos. Sci. Technol. 58 (1) (1998) 1–8, doi:10.1016/S0266-3538(97)00075-4.
[37] L. Melin, Fatigue testing and buckling characteristics of impacted composite specimens, Int. J. Fatigue 24 (2–4) (2002) 263–272, doi:10.1016/S0142-1123(01)00081-0.
[38] T. Yokozeki, A. Kuroda, A. Yoshimura, T. Ogasawara, T. Aoki, Damage characterization in thin-ply composite laminates under out-of-plane transverse loadings, Compos. Struct. 2010 (93) (2010) 49–57, doi:10.1016/j.compstruct.2010.06.016.
[39] B. Kötter, P. Polyak, J. Körbelin, B. Fiedler, Influence of ply thickness on failure initiation, propagation and mechanical properties in CFRP laminates, 2018.
[40] A. D3039-00, Standard test method for tensile properties of polymer matrix composite materials, 2000.
[41] A. D6641-16, Test method for compressive properties of polymer matrix composite materials using a combined loading compression (CLC) test fixture, 2016.
[42] ASTM D6484-04, Standard test method for open-hole compressive strength of polymer matrix composite laminates, 2004.
[43] ASTM D7136-05, Measuring the damage resistance of a fiber-reinforced polymer matrix composite to a drop-weight impact event, 2005.
[44] J. Cugnoni, R. Amacher, S. Kohler, J. Brunner, E. Kramer, C. Dransfeld, W. Smith, K. Scobbie, L. Sorensen, J. Botsis, Towards aerospace grade thin-ply composites: effect of ply thickness, fibre, matrix and interlayer toughening on strength and damage tolerance, Compos. Sci. Technol. 168 (2018) 467–477, doi:10.1016/j.compscitech.2018.08.037.
[45] ASTM D3410-03, Standard Test Method for Compressive Properties of Polymer Matrix Composite Materials with Unsupported Gage Section by Shear Loading, 2003.
[46] S. Abrate, Impact engineering of composite structures, Courses and lectures, 526, Springer, Vienna and New York, 2011.
[47] ASTM D7137-05, Test method for compressive residual strength properties of damaged polymer matrix composite plates, 2005. doi:10.1520/D7137_D7137M-05.